JOURNAL OF PROPULSION AND POWER
Vol. 14, No. 1, January–February 1998

Experimental Analysis of the Turbulent Shear Stresses for Distorted Supersonic Boundary Layers

Joel J. Luker,* Chad S. Hale,* and Rodney D. W. Bowersox†
U.S. Air Force Institute of Technology, Wright–Patterson Air Force Base, Ohio 45433-7765

An experimental analysis of the turbulent shear stresses for a supersonic boundary layer distorted by streamline curvature-induced pressure gradients was performed using laser Doppler velocimetry. Four pressure-gradient flows were examined: a nominally zero-pressure-gradient case ($M = 2.8$, $Re_\theta = 1.1 \times 10^4$, $\beta = 0.02$); a favorable-pressure gradient ($M = 2.9$, $Re_\theta = 1.5 \times 10^4$, $\beta = -0.5$); an adverse-pressure gradient ($M = 2.7$, $Re_\theta = 1.2 \times 10^4$, $\beta = 0.9$); and a successive-pressure gradient ($M = 2.5$, $Re_\theta = 1.2 \times 10^4$, $\beta = -1.0$, following a region of $\beta = 0.9$). For the favorable-pressure gradient, the turbulent shear-stress levels across the boundary layer decreased by 70–100%, as compared to the zero-pressure-gradient boundary layer. For the adverse-pressure gradient, a 70–100% increase was observed. For the combined-pressure gradient, the shear stresses returned to values similar to the zero-pressure-gradient flow. A new pressure gradient parameter was found to correlate well with the peak shear-stress amplification. It was also postulated that the shear-stress amplifications were in part the result of the nonuniform bulk dilatation/compression and streamline divergence/convergence, implying a forcing phenomena that influenced the statistical $\overline{u'v'}$ correlation. The combined-pressure-gradient flow demonstrated that the turbulent structure adjusts relatively rapidly to the distortion. Numerical simulations of the mean velocity obtained with a k-ω turbulence model were found to agree very well with the present data. With the exception of the zero-pressure-gradient flow, the magnitudes of the turbulent shear stresses were not accurately reproduced; however, correct trends were predicted.

Nomenclature

B	= pressure gradient parameter
d	= distortion parameter, $e/\partial\bar{u}/\partial y$
e	= extra strain rate
H	= δ^*/θ
I	= impulse, $\int_{edt}$
k	= turbulent kinetic energy
L_i	= length of interaction region
M	= Mach number
Re	= Reynolds number
u, v, w	= velocity components
u^*	= friction velocity $(\sqrt{\tau_w/\rho_w})$
y^+	= $\rho_w u^* y/\mu_w$
β	= $\delta^*/\tau_w\, dp/dx$
δ	= boundary-layer thickness
δ^*	= kinematic displacement thickness
θ	= kinematic momentum thickness
τ	= shear stress
ϕ	= local deflection angle

Subscripts

e	= boundary-layer edge
p	= bulk compression or dilatation
t	= total condition
w	= wall
ϕ	= wall deflection

Superscripts

0	= inflow condition
$''$	= Favre fluctuating component
$'$	= Reynolds fluctuating component
$-$	= Reynolds mean component

Introduction

SUPERSONIC flow over curved surfaces has many practical applications, for example, exterior aerodynamic lifting surfaces, supersonic aircraft engine inlet compression ramps, supersonic turbofan, and supersonic nozzle flows. Because of the large number of practical usages, these flows have been the subject of much investigation.[1–25] However, as discussed by Bradshaw[1] and Spina et al.,[2] the understanding of the fundamental physical processes remains uncertain. Hence, investigations of these flows have important theoretical implications. The primary reason for the lack of understanding of supersonic flows with pressure gradient effects has been attributed to the scarcity of accurate experimental data. As indicated by Spina et al.,[2] acquiring quality data is very difficult in these flows. A recent survey by Settles and Dodson[3] exemplifies the current state of affairs. After reviewing over 100 shock/boundary-layer interaction studies with a freestream Mach number greater than 3.0, 19 passed a criterion that Settles and Dodson deemed necessary for turbulence model development.

A second factor contributing to the lack of understanding of these flows is the inability of current and foreseeable near-future computational techniques to perform direct numerical simulation of the turbulence for high Reynolds number flows. Many of the terms, e.g., the static pressure-velocity fluctuation correlations, that arise in the equations governing the transport of the second-order turbulent correlations are currently not measurable. Hence, the experimental and computational limitations couple to make the study of high-speed high-Reynolds number turbulence particularly arduous and highly empirical.

Since 1961, researchers and engineers have enjoyed the simplifying ramifications of Morkovin's hypothesis.[5] However,

Received Dec. 13, 1996; revision received July 28, 1997; accepted for publication Aug. 5, 1997. This paper is declared a work of the U.S. Government and is not subject to copyright protection in the United States.

*Research Assistant, Graduate School of Engineering, Department of Aeronautics and Astronautics.
†Assistant Professor, Graduate School of Engineering, Department of Aeronautics and Astronautics; currently Assistant Professor, Department of Aerospace Engineering and Mechanics, University of Alabama, Tuscaloosa, AL 35487-0280. Senior Member AIAA.

Spina et al.[2] suggest that the effects of compressibility become important at Mach numbers lower than originally believed. The measurements of Morkovin,[6] Miller et al.,[7] and Bowersox and Buter[8] indicated that the compressible turbulence term (i.e., $\overline{\rho' v'}$) measured across supersonic boundary layers was dramatically influenced by favorable and adverse-pressure gradients. In addition, the compressible turbulence contribution to the Reynolds shear stress has been shown to be significant[6–8]; i.e., $\bar{u}\overline{\rho' v'}/\bar{\rho}\overline{u' v'} > 1.0$. On the other hand, Smith and Smits[4] observed that turbulence models based on Morkovin's hypothesis[6] were adequate for predicting the effects of the pressure gradient and streamline curvature on turbulent Reynolds shear stress.

Although the flow physics associated with a supersonic turbulent boundary layer subjected to a pressure gradient are not currently fully understood, many of the salient features have been well characterized. For example, many of the observed differences between distorted supersonic and subsonic boundary layers can be explained in terms of the fluid property changes across the boundary layer.[2,4] However, supersonic flows possess phenomena that do not have incompressible counterparts. For example, wave (expansion or compression) boundary-layer interactions, where the longitudinal pressure gradients can lead to compression or dilatation, which in turn affect the velocity pressure and density fluctuations, are not present in subsonic flow.

There are basically two ways to generate a pressure gradient in supersonic flow, wave–boundary-layer interaction and streamline curvature. For the case of a curved wall, it is difficult to separate the effects of streamline curvature and pressure gradient on the turbulent flow properties; however, for an imposed wave, the streamline deflection angle is usually very small; hence, the effects of pressure gradient can be isolated.[4] The differences between the two methods make characterizing the strength of the perturbation tenuous. Smith and Smits[4] suggested that the Clauser pressure-gradient parameter is not a sufficient characterization parameter for supersonic flow.

Bradshaw[1] concluded that the mean dilatational strain rate directly affects the turbulence to an extent much higher than that expected from the terms in the Reynolds stress transport equations that contain the extra strain rates explicitly. Bradshaw also proposed that the turbulent energy dissipation terms should be divided by a factor given by $F = 1 + \alpha d$, where d is the distortion defined as the ratio of the extra strain rate to the primary $\partial\bar{u}/\partial y$ velocity gradient. The constant α is on the order of 10. As noted by Bradshaw, the factor F is not a law of nature; instead it represents an empirical correction that has been successfully used to predict the effects of suddenly applied curvature, lateral divergence, and dilatation. In any event, the distortion parameter d has been used as a convenient means to classify a pressure gradient. A distortion is generally considered mild if $d_{\max} \approx 0.01$ and strong if $d_{\max} \approx 0.1$. If the distortion is applied for a time that is comparable to an eddy lifetime, then the impulse parameter I, the time-integrated strain rate, may be a better choice.[4] For an impulsive perturbation resulting from a region of bulk compression, $I_p = \ell n(p2/p1)/\gamma$.[4,9] For an impulse as a result of curvature, $I_\phi = \Delta\phi$.[10] Even though the interactions between the strain rates are most likely nonlinear, the linear addition of the perturbation strengths is usually accepted for crude comparisons among different flows.[4]

When a streamwise adverse-pressure gradient is imposed on a supersonic boundary layer, the flow is distorted by both the effects of pressure gradient and bulk compression. While few turbulence measurements have been made in such flows, the mean flowfields have been well documented.[2] For a supersonic boundary layer where the subsonic region is small compared to the boundary-layer thickness, the adverse-pressure gradient causes the skin friction to increase and the boundary-layer thickness to decrease. As discussed in Spina et al.,[2] this counterintuitive behavior arises in supersonic flow as a result of the density increasing more rapidly than the velocity decreases through the pressure gradient region.

In general, adverse-pressure gradients have been shown to have destabilizing effects on turbulent boundary layers, where the turbulent fluctuation properties increase in magnitude. A number of studies have been performed where the adverse-pressure gradient was generated by imposing a wave (compression and shock) onto a boundary layer.[11–15] Because these flows experienced minimal streamline curvature, the sole effects of the adverse-pressure gradient could be assessed. As reported in Bradshaw,[1] Spina et al.,[2] and Smith and Smits,[4] the Reynolds shear stresses are considerably amplified by the pressure gradient. For the case of Fernando and Smits,[14] the Reynolds shear stress was amplified by 220% for an impulse of $I_p = 0.46$ applied over a distance of 7.0 boundary-layer heights. In addition, for moderate pressure gradients, van Driest scaling[16] has been found to hold.[4]

Concave streamline curvature can be used to generate an adverse-pressure gradient.[17–20] However, as mentioned earlier, it is difficult to separate the destabilizing effects of the concave streamline curvature from those of the adverse-pressure gradient. Thomann[17] found that the 20-deg concave curvature (with the pressure gradient eliminated) increased the wall heat transfer by 20%. The data summarized in Smith and Smits[4] also suggest that the amount of amplification of the Reynolds shear stress depends not only on the magnitude of the streamline curvature and pressure gradient, but also on the spatial extent of the distortion. Smith and Smits found that the more rapid the perturbation, the higher the amplification. The peak Reynolds shear stress was amplified by 200% for a pressure gradient with $I_p = 0.46$, $I_\phi = 0.14$, and a length of 7.0 boundary-layer heights. For a similar magnitude pressure gradient applied more rapidly (1.4 boundary-layer heights), the peak amplification was 390%. Hence, in addition to the impulse function and Clauser parameter, the length of the pressure-gradient region is also required for characterizing pressure gradients.

The number of investigations of favorable-pressure-gradient flows is dramatically fewer than those of adverse-pressure gradients.[6,17,21–25] Of the available reports, only the results of Arnette et al.[25] provide turbulent shear stress data. However, other studies have found that the axial turbulent shear stress decreased by 70–90% for I_p and I_ϕ values $\in (-0.5, -1.0)$ and $(-0.2, -0.3)$, respectively.[2,4] Hence, an imposed expansion results in a bulk dilatation and an expansion of the supersonic stream tubes, which have been deemed to be a stabilizing phenomenon, where the magnitude of the turbulent fluctuation properties decreases. Relaminarization of part of the boundary layer is believed possible if the pressure gradient is strong enough. Further, Thomann[17] demonstrated that convex curvature, with the pressure gradient removed, is also stabilizing. Smith and Smits[22] and Dussauge and Gaviglio[23] estimated, using a rapid distortion analysis, that the majority of the turbulence reduction was an effect of the mean bulk dilatation.

Arnette et al.[25] showed that the overall magnitude of the kinematic Reynolds shear stress was dramatically decreased across the entire boundary layer for 7.0 and 14.0 deg centered and gradual expansions. They further defined an apparent reverse transition, where the normal energy transfer from the mean flow has been reversed, to describe a sign changing of the Reynolds shear stress for the 14-deg expansions.

Successive, or combined, pressure-gradient flows have received very little attention.[4,26] In the Smith and Smits[4] study, the response of the boundary-layer properties to the successive distortions ($I_p = 0.35$ and $I_\phi = 0.92$, followed by $I_p = -0.35$ and $I_\phi = -0.92$) was found to occur rapidly. Smith and Smits also noted that the turbulent stress levels returned to nearly the upstream values at the exit of the second perturbation. However, further downstream, an undershoot of the turbulence levels suggested an underdamped second-order response.[4]

With the exception of the laser Doppler velocimetry (LDV) study of Arnette et al.,[25] hot-wire anemometry has been almost exclusively used to characterize the turbulent structure of these distorted boundary-layer flows. However, to deduce the kinematic turbulent shear stress from this technique, an ad hoc assumption concerning the static pressure fluctuation field is required, e.g., $p' \approx 0$. For zero-pressure-gradient boundary layers and free shear layers, this assumption appears to provide reasonable results.[8] However, in the presence of a pressure gradient or distortion, the validity has not been established.

The purpose of the present study was to examine experimentally, using LDV, the turbulent shear stresses of supersonic boundary layers, which were distorted by streamline-curvature-driven pressure gradients. The experimental results are compared to numerical predictions using a k-ω two-equation turbulence model.[27] Four pressure gradient flows were examined: 1) a nearly zero ($\beta = 0.02$) pressure gradient (ZPG) baseline case was documented for comparative purposes; 2) a favorable-pressure gradient (FPG, $\beta = -0.5$, $I_p = -0.13$, and $I_\phi = -0.14$) associated with flow over a convex wall; 3) an adverse-pressure gradient (APG, $\beta = 0.9$, $I_p = 0.09$, and $I_\phi = 0.12$) created with a concave wall; and 4) a combined, or successive, pressure gradient (CPG) model that had a convex surface following a concave wall ($\beta = -1.0$ following a region of $\beta = 0.9$, $I_p = -0.21$ following 0.09, and $I_\phi = -0.04$ following 0.12). The measurements include the wall pressure, the mean velocity profiles, the mean strain rates ($\partial\bar{u}/\partial y$, $\partial\bar{u}/\partial x$, $\partial\bar{u}/\partial z$, $\partial\bar{v}/\partial y$, $\partial\bar{v}/\partial x$, and $\partial\bar{v}/\partial z$), and the kinematic turbulent shear stresses ($-\overline{u'v'}$).

Experimental Apparatus

Facilities

All tests were performed in the U.S. Air Force Institute of Technology's pressure–vacuum supersonic wind tunnel (Fig. 1). The freestream Mach number was 2.9, with a ± 0.02 variation across the test section. The settling chamber pressure and temperature were maintained at 2.0 ± 0.03 atm and 294 ± 2 K, respectively, for all tests. The freestream Re/m was 15×10^6. The freestream turbulent kinetic energy was 0.016% of the mean specific kinetic energy. The test section was 6.35×6.35 cm in cross section. The coordinate system was defined such that x was positive in the streamwise direction, and the origin was located at the nozzle throat. Because all of the measurements were made normal to the tunnel ceiling, y was defined as positive down, and it was zero at the test section ceiling; z completed the right-hand system.

The curved-wall sections were built into the tunnel ceiling as shown in Fig. 1, and the contours started at $x = 65.08$ cm. The curved-wall contours were generated to match a cubic polynomial $\Delta h = a_0 + a_1\Delta x + a_2\Delta x^2 + a_3\Delta x^3$, where Δh (cm) was relative to the tunnel ceiling, and Δx (cm) $= x - 60.0$. The coefficients for each model are given in Table 1. The tunnel height above the lower floor is shown in Fig. 2. The FPG model is given by the dashed line. For this model, the measurements were acquired normal to the curved wall at $x = 71.5$ cm. The APG and CPG flows were generated with the same model, which is indicated by the solid line. The measurements normal to the curved wall were acquired at $x = 68.0$ and 71.0 cm for the APG and CPG models, respectively. The

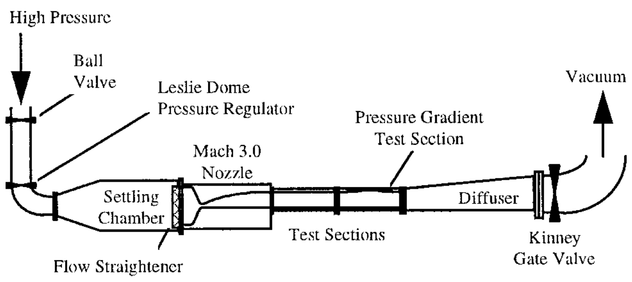

Fig. 1 Schematic of the AFIT pressure–vacuum supersonic wind tunnel.

Table 1 Model contours

Model	$a_0 \times 1$	$a_1 \times 10$	$a_2 \times 100$	$a_3 \times 1000$
FPG	−0.2078	0.8970	−0.9476	−0.03598
CPG	1.186	−5.410	7.478	−2.800

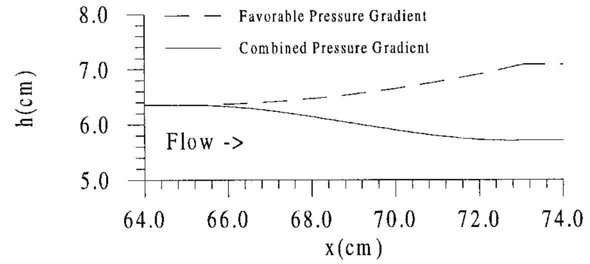

Fig. 2 Schematic of curved-wall contours.

zero-pressure-gradient data were also taken at $x = 71.5$ cm downstream of the nozzle throat. These measurement locations were nominally 3500 momentum thickness heights downstream of the nozzle exit, and the boundary layer has been documented to be in a state of equilibrium.[8]

Instrumentation

A Dantec brand 57N Enhanced BSA two-component LDV system, with a 300-mW argon–ion laser, was used for the present experiment. The $1/e^2$ beam diameter was 0.82 mm. The green beams (514.5 nm) and blue beams (418.0 nm) were aligned parallel and perpendicular to the model walls, respectively. This was done to avoid the angular bias reported in Ref. 18. A 40-MHz frequency shift was applied across both the green and blue components. A 600-mm focal-length transmitting lens was used; this provided a 0.276-mm-diam control volume that was 0.9 cm long (along the z axis). Because of the increased intensity of the scattered light, forward scattering was used. However, to prevent damaging the photomultiplier tubes, the system was operated 3.5 deg off axis. The Dantec three-dimensional traverse system was used. The rated accuracy was ± 13 μm for 600 mm of movement. The flow was seeded by injecting 0.6-μm-diam particles of olive oil along the centerline of the tunnel upstream of the flow straighteners within the stilling chamber. The particles were generated with a TSI brand Six Jet Atomizer.

LDV provided direct measurements of the mean velocity ($\bar{u}$ and $\bar{v}$) and the kinematic Reynolds shear stress, i.e., $\tau_{xy}/\bar{\rho}\bar{u}^2 = -\overline{u'v'}/\bar{u}^2$. For homogenous gaseous flows, the Favre-averaged turbulent shear stress, which is almost universally used in modern numerical prediction formulations, has been shown to reduce to the kinematic shear stress given earlier.[8] Random error analysis indicated a ± 9.0 and ± 8.0% uncertainty in the mean velocity and Reynolds shear stress, respectively. The unusually large mean velocity uncertainty estimate resulted from the probe position uncertainty (0.01 mm) and the very large near-wall velocity gradient. In the freestream, the mean velocity uncertainty was estimated as 2.0%.

Surface pressure measurements were obtained by instrumenting the model walls with a series of 1.59-mm-diam pressure taps. Endevco brand ± 1.02-atm pressure transducers were incorporated to monitor the pressure. Random error analysis indicated a ± 2.0% uncertainty in the surface pressure measurements.

Results and Discussion

Mean Flow Results

Presented in Fig. 3 are the wall pressure distributions for the two models. As indicated, the FPG model experienced a favorable-pressure gradient over the complete model. The APG/CPG model experienced an adverse-pressure gradient

Table 2 Summary of local boundary-layer and pressure-gradient parameters

Model	M_e	δ, mm	δ*/δ	θ/δ	H	Re_θ	C_f[a]	β	d_{max}	I_P[b]	I_θ[c]	L_i/δ_O[d]	$I_T/(L_i/\delta_O)_T$
ZPG	2.79	9.9	0.062	0.050	1.24	1.1×10^4	0.0016	0.02	0.02	0.10	0	27.9	0.003
FPG	2.91	11.9	0.075	0.056	1.34	1.5×10^4	0.0011	−0.5	0.14	−0.13	−0.14	8.1	−0.03
APG	2.72	9.1	0.083	0.074	1.12	1.2×10^4	0.0022	1.0	0.14[e]	0.09	0.12	4.0	0.04
CPG[f]	2.51	7.5	0.075	0.060	1.25	1.2×10^4	0.0010	−0.9	0.16	−0.21	−0.04[g]	4.1	−0.002

[a]Estimated via the Couette flow assumption. [b]Based on measured boundary-layer edge pressure. [c]Based on local wall inclination. [d]Length of curved-wall model, $\delta_O = \delta_{ZPG}$. [e]Based on transverse extra strain rates only. [f]Downstream of the above APG flow. [g]Relative to the model inflection point.

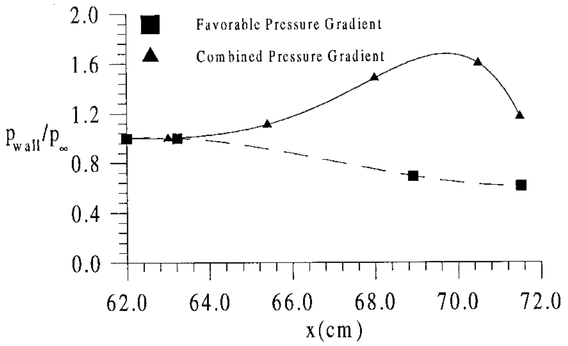

Fig. 3 Wall pressure contours (uncertainty: ±2%).

followed by a favorable-pressure gradient. The inflection point for the model was located at $x = 68.93$ cm, which is in agreement with the peak pressure, as indicated by the polynomial fit.

The measured boundary-layer parameters are summarized in Table 2, and random error estimates for all of the data used to generate Table 2 are discussed in the preceding text.[28,29] The zero-pressure-gradient freestream conditions ($x = 71.5$ cm) were used as the reference upon which the effects of the pressure-gradient/streamline curvature could be assessed. The edge Mach number was estimated from the measured velocity (LDV) and assuming an adiabatic flow in the freestream. Because the probe volume traversed normal to the wall, the indicated change in Mach number, relative to the ZPG case, was less than that estimated using the Prandtl–Meyer theory and the local wall inclination; i.e., as the control volume traversed across the boundary layer into the freestream, it moved across successive compression waves in an upstream orientation. The importance of this observation is that the pressure gradient along the boundary-layer profile varies transversely. Table 2 also shows that the kinematic boundary-layer thickness increased for the FPG flow and decreased for the APG case, which was the expected trend.[2] Interestingly, the boundary-layer thickness for the CPG model was significantly reduced as compared to the upstream APG region result. This is expected to be a result of the outer region of the boundary-layer profile only experiencing a fraction of the expansion because of convex curvature.

The boundary-layer shape factor H, summarized in Table 2, was interesting in the sense that the trends were opposite of those expected for incompressible boundary layers. The zero-pressure-gradient value of $H = 1.24$ was in very good agreement (well within the uncertainty as a result of the experimental data scatter as seen in Fig. 4) with the predicted value of 1.22, which was estimated from the incompressible Law of the Wall with Coles wake function.[30,31] Note that the simpler one-seventh power law of Prandtl yielded a value of 1.28. To predict the effects of pressure gradient, the Coles wake function was estimated as a function of the Clauser parameter using the empirical curve fit given in White.[31] The values of H were estimated as 1.12 and 1.41 for $\beta = -0.5$ and 1.0, respectively. Comparing to Table 2, it can be seen that the overall magnitudes were consistent, but the trend was reversed. This apparent contradiction was a result of the incompressible flow assumption used in the estimate. Recall from the Introduction that the effects of the density variation across the flow are very important for flows that are supersonic over most of the boundary layer,[2] as was the case for the present study.

Figure 5 shows the axial velocity profiles plotted with van Driest scaling for each of the four flow conditions. The minimum measured y^+ locations for each data set were estimated as 100, 50, 100, and 200 for the zero, favorable, adverse, and combined-pressure-gradient boundary layers, respectively. As indicated in Fig. 5, the inner region of the boundary layer was reasonably correlated with the use of van Driest scaling. This is consistent with the incompressible result that the inner region of the boundary layer is essentially unaffected by a pressure gradient.[30]

The present experimental results are compared to the numerical simulations obtained with the k-ω turbulence model[27,33] in Fig. 4. As can be seen, the agreement was very good for all four cases. Based on the conclusions in Smith and Smits[4] concerning the use of Morkovin's hypothesis,[5] this agreement was not overly surprising. In addition, Fig. 4a compares the velocity profiles obtained using conventional mean-flow probes. The combined usage of a pitot pressure and a 10-deg, semivertex angle, cone-static probe resulted in a direct measurement of the Mach number across the boundary layer. The conventional probe velocity profile in Fig. 4a was computed from the Mach number data with the assumption of a constant total temperature. Random error analysis indicates a 3.0% uncertainty. As indicated in Fig. 4a, the agreement between the two techniques was excellent, except very near the wall where the mean flow probe dimensions were on the same order as the distance from the wall.

Because the LDV measurements were obtained in the logarithmic portion of the boundary layer, the wall shear stress was estimated by applying the Couette flow assumption in the near-wall region; i.e., $\tau_{xy}^T = \tau_w + (\mathrm{d}p_w/\mathrm{d}x)y$. The skin friction C_f values summarized in Table 2 were estimated with this relation using the measured turbulent shear stresses (discussed in the Turbulence Results section) and the pressure data in Fig. 2. In an attempt to validate the present results, the van Driest II skin friction correlation[16] was used to estimate the wall shear stress. To perform the analysis, it was assumed that the zero-pressure-gradient flow could be modeled as a flat plate with its origin starting at $x = 0$. The results from that analysis agreed to within 4.3%, which was well within the expected ±10% uncertainty of the correlation.

The Clauser[32] pressure gradient parameter β was also estimated from the measured data as given in Table 2. Because of the natural growth of the tunnel boundary layers, a very slight adverse pressure increase ($\beta = 0.02$) existed. However, this was considered negligible, and these data were used as the zero-pressure-gradient comparison case. As can be seen, the favorable-pressure gradient was also mild ($\beta = -0.5$) in the sense of the Clauser parameter. The pressure gradients associated with the adverse and combined flows ($\beta \approx \pm 1.0$) were stronger than that of the favorable-pressure gradient. However, β values of ±1.0 are also generally considered to be mild. As mentioned in the Introduction, the use of the Clauser parameter may not be the most suitable choice to quantify the pressure gradient. Hence, d was also estimated for the four flows here. Those results are summarized in Table 2. The distortion parameter values of order 0.1 indicated strong pressure gradients, which contradicts the classification that re-

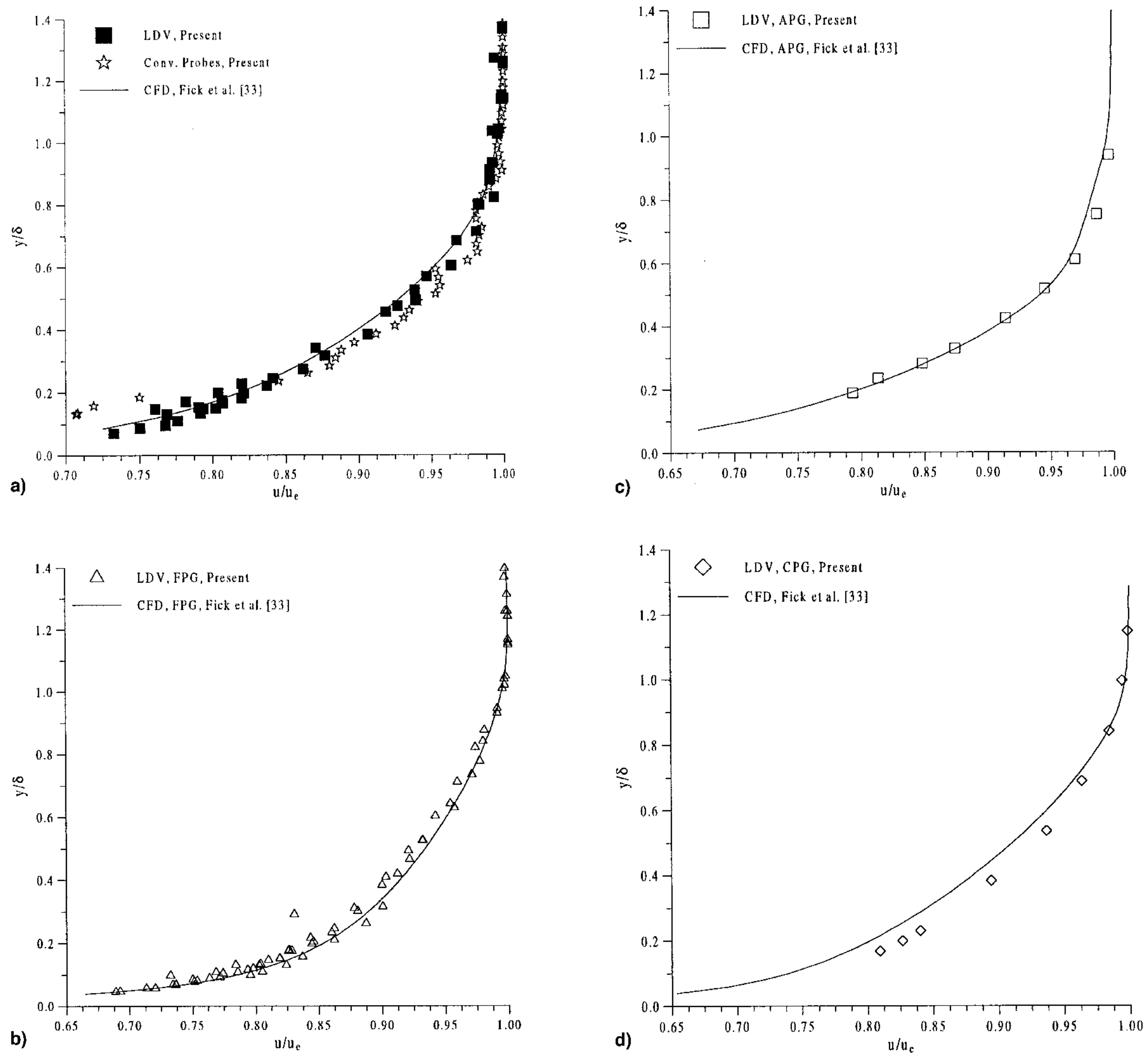

Fig. 4 Comparison of predicted (k-ω) and experimental velocity profiles: a) ZPG, b) FPG, c) APG, and d) CPG.

sulted from the Clauser parameter. Also, the impulse functions (I_p and I_ϕ) were computed. These values were based on the local measured properties in Table 2. As discussed earlier, the pressure gradient varies across the boundary layer. Thus, a range of I_p is present. Hence, an equally valid method for estimating I_p would be to use the pressure estimated by the Prandtl–Meyer theory and the local wall inclination. Although the choice is somewhat arbitrary, the effects on the magnitude of I_p can be pronounced (see Table 3). The length of the interaction affects the magnification of the turbulent shear stresses. Hence, those values are also summarized in Table 2.

The difficulty associated with classifying the strength of a pressure gradient is clearly depicted in the data summarized in Table 2 and the earlier discussion. For example, for the ZPG case I_p, which was estimated based on data acquired at x = 44 and 71.5 cm, was slightly higher in magnitude than that for the APG model. Hence, by that criterion, the flow experienced a strong pressure gradient. However, all other indicators would imply that the ZPG model experienced a negligibly small pressure gradient. Comparison of the upstream (x = 44 cm) and downstream turbulence data indicated that the turbulent shear stresses were unaffected.[8] Thus, at a minimum, all of the pressure gradient parameters summarized in Table 2 are required to qualitatively assess the strength of the pressure gradient.

In an effort to present a global parameter that has the form of a nondimensional pressure gradient and uses the data that are readily available, the following definition is proposed:

$$B = \frac{I_T}{\left(\frac{L_i}{\delta_0}\right)_T} \equiv \frac{\sum (I_p + I_\phi)}{\sum \left(\frac{L_i}{\delta_0}\right)} \tag{1}$$

The summation is included for the successive pressure gradient models, where it is assumed in Eq. (1) that the total effect of the pressure gradient can be crudely represented by a simple summation. The form of the parameter in Eq. (1) is reminiscent of the Clauser pressure-gradient parameter; however, the wall shear stress, which is usually not reported, is removed. The new parameter estimates for the present flows are summarized in the last column of Table 2. The utility of this parameter, along with all of the others in Table 2, will be discussed in more detail in the following text, when comparing the turbulent shear stress profiles.

The mean transverse strain rates were estimated for all four models. Axial and span strain rates for the ZPG, FPG, and CPG models were acquired using the experimental measurement stencil shown schematically in Fig. 6. Hale[28] and Luker[29] provide detailed information concerning the measurement procedure. Random error analysis indicated a nominal uncertainty of roughly ±15.0% for all of the strain rates. The trans-

Table 3 Comparison of the effects of pressure gradient on turbulent shear stresses

Flowfield parameter	FPG, Present/ Arnette et al.[25]	APG, Present/ Jayaram et al.[18]	CPG, Present/ Smith and Smits[4]
M_e	2.9/3.0	2.9/2.9	2.9/2.9
$Re_\theta \times 10^3$	15/25	12/78	12/78
R_c/δ_O	49/50	68/50	(68/29)/(15/15)
L_i/δ_O	8.1/6.0	4.0/7.0	(4.0/4.1)/(0 − 12/——)
I_p[a]	−0.47/−0.41	0.35/0.46	(−0.47/0.29)/(0.92/−0.92)
I_ϕ	−0.14/−0.12	0.12/0.14	(0.12/−0.04)/(0.35/−0.35)
$I_T/(L_i/\delta_O)_T$	−0.08/−0.09	0.1/0.09	−0.006/0.0
Maximum amplitude,[b] %	−100/−100	100/100	30/≈0[c]

[a]Based on Prandtl–Meyer theory and local wall inclination.
[b]$(\tau_{xy} - \tau^0_{xy})/\tau^0_{xy}$.
[c]Based on discussion in Smith and Smits.[4]

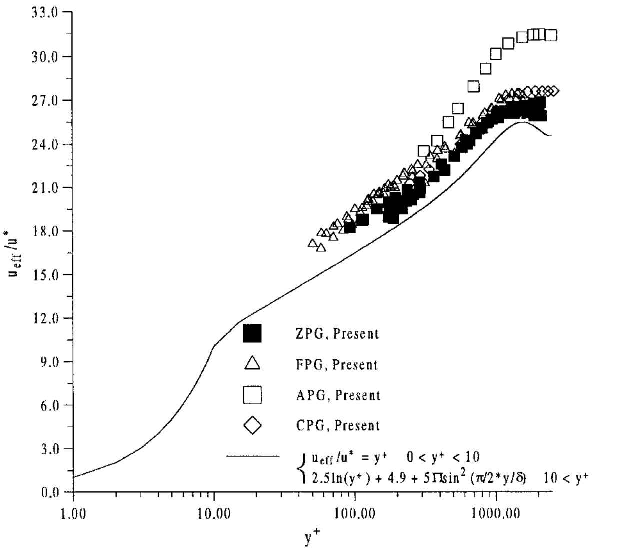

Fig. 5 Velocity profiles with van Driest scaling (total uncertainty: ±19.0%).

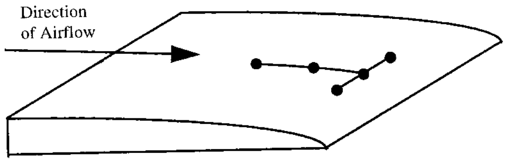

Fig. 6 Schematic of the strain rate measurement stencil (shown for the FPG model).

verse, axial, and spanwise strain rate measurements are shown in Figs. 7a, 7b, and 7c, respectively.

The principal strain rates (Fig. 7a) were reasonably unaffected by the pressure gradient. The peak transverse strain rates for the three pressure gradients were estimated from Fig. 7a ($y/\delta = 0.3$–0.4) as $0.07\delta/U_e$, $-0.07\delta/U_e$, and $0.07\delta/U_e$, for the FPG, APG, and CPG models, respectively. The peak FPG and CPG axial strain rates ($y/\delta = 0.3$–0.4) were estimated from Fig. 7b as $-0.04\delta/U_e$ and $0.08\delta/U_e$, respectively. Values below $y/\delta = 0.2$ were not included in the preceding estimates because of possible errors as a result of laser beam reflections off of the tunnel ceiling. The data in Fig. 7c demonstrate that the flow was two dimensional. The peak distortion magnitudes summarized in Table 2 were estimated from these data.

Turbulence Results

Figure 8 shows a comparison of the present zero-pressure gradient turbulent shear stress measurements to the Mach 2.9 boundary-layer results of Miller et al.,[7] Robinson et al.,[34] Elena and LeCharme,[35] and Johnson and Rose,[36] and the $M = 0.0$ data of Klebanoff.[37] The overall qualitative agreement of the present results to the previous data is quite good. Because of the uncertainties associated with the wall shear stress, boundary-layer thickness, and turbulent shear stresses, the relatively large scatter in Fig. 8 is reasonable.

The kinematic turbulent-shear-stress profiles for the four pressure gradients are presented in Fig. 9. Also shown are the numerical predictions using the k-ω model described in Wilcox.[27] Details concerning the numerical methods can be found in Fick et al.[33] As anticipated, the agreement between the numerical and experimental results for the zero-pressure-gradient flow was very good.

When compared to the ZPG model, the FPG turbulent shear stresses were dramatically reduced (nominally 70 to 100%). This result agrees with the perceived stabilizing effect of both the convex curvature and favorable-pressure gradient. It was estimated that for the 7-deg gradual expansion case of Arnette et al.,[25] which best matches the flow conditions here, the shear stresses also decreased by roughly −70 to −100%. The impulse-based pressure gradient parameters discussed earlier were estimated from their data using the Prandtl–Meyer theory and the local wall inclination. A comparison to the present study is given in the first column of Table 3, where the pressure gradient parameters for the present flow were estimated in the same way. As can be seen, the flowfields and effects on the turbulent shear-stress peak amplifications were very consistent between the two studies.

The near-zero and slightly negative shear stress values in the outer region of the boundary layer is a second important effect of the convex curvature-driven pressure gradient (Fig. 9). Arnette et al.[25] observed the same phenomena. They reasoned that a reverse transition process was occurring, where the turbulent kinetic energy was observed by the mean flow. Although the turbulent kinetic energy levels for both the Arnette et al.[25] and the present study[29] were reduced as a result of the favorable-pressure gradient, they were not nearly as affected as the shear stress. Hence, it is expected that an additional phenomena may be in part responsible for dramatic effect on the turbulent shear stresses. It is important to recall that the kinematic turbulent shear stress is a statistical moment that appears in the Reynolds-averaged momentum equation as a result of the nonlinear inertia terms. With this the processes of bulk dilatation and streamline divergence can be postulated to behave as forcing functions that drive the $\overline{u'v'}$ correlation positive. Apparently, if the process is strong enough, the pressure-gradient forcing function can overcome that of the mean velocity gradient across the boundary layer.

A simple momentum transfer argument indicates that the velocity gradient across the boundary layer results in a positive shear stress. Consider a fluid clump in a ZPG boundary layer that moves in the positive transverse direction (i.e., $\Delta v > 0$), it will carry with it a lower axial velocity, hence, $\Delta u < 0$. Therefore, the velocity correlation $(\overline{u'v'})$ would be negative. Hence, the velocity gradient across the boundary layer acts as a forcing function that results in a positive turbulent shear stress.[30]

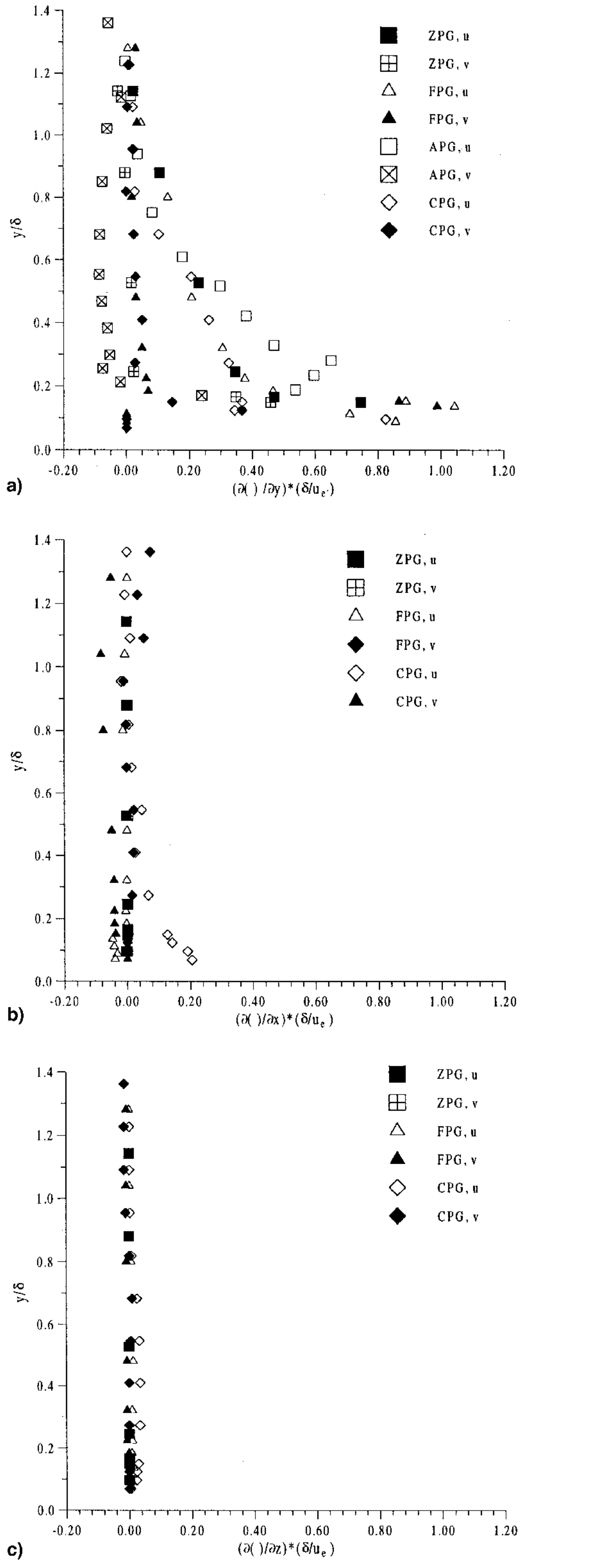

Fig. 7 Measured strain rates: a) transverse, b) axial, and c) spanwise.

Now, if the effects of the expansion emanating from the wall (i.e., nonuniform bulk dilatation and streamline divergence) are included in the preceding argument, it can be shown that the expansion associated with the favorable-pressure gradient can result in reduced (or even negative) turbulent shear stresses. Consider the fluid clump moving in the positive transverse direction normal to the wall. As the clump moves up, i.e., $\Delta v > 0$, it will cross successive expansion waves in an upstream

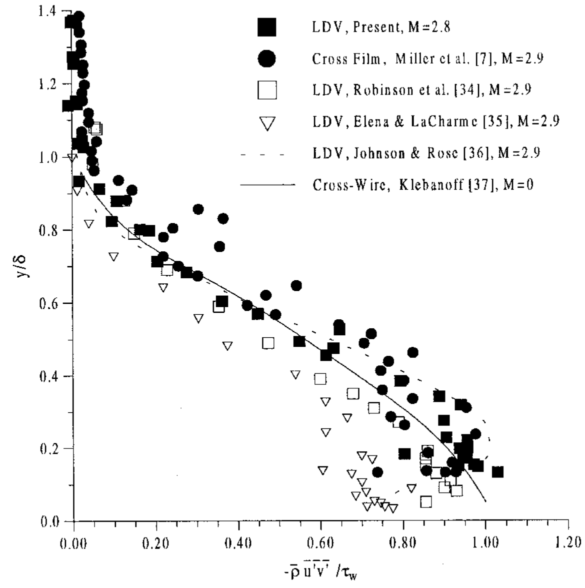

Fig. 8 Zero-pressure-gradient turbulent shear-stress profiles.

orientation, i.e., the boundary layer experiences more expansion as the wall is approached. Hence, neglecting the boundary-layer effects, $\Delta u > 0$ as a result of the expansion, i.e., the fluid clump will carry with it a higher axial velocity. Thus, the net change in axial velocity Δu will depend on the magnitude of the velocity gradient across the boundary layer ($\Delta u < 0$) and that caused by expansion fans $\Delta u > 0$. Therefore, the turbulent shear-stress value will decrease, and perhaps be negative for the favorable-pressure gradient flow. The expansion wave effects are probably most pronounced in the outer region of the boundary layer, where the velocity gradients are relatively small and the expansions are relatively strong, i.e., higher Mach number. The FPG data in Fig. 9 conform to this model.

Comparing the numerically predicted shear stresses to the FPG data, the magnitude was significantly overpredicted ($\approx$200%), but the correct trend was captured. In light of the discussion in Bradshaw,[1] the ability of the k-ω model to capture the trend was not surprising. In addition, it was not expected that the model would predict the negative shear stresses in the outer half of the boundary layer. Referring back to Fig. 4, this would require a negative eddy viscosity, which is impossible for the k-ω model to predict.

The APG shear stresses were significantly increased (75–100%) as a result of the destabilizing concave curvature and adverse-pressure gradient. Following the same argument as in the preceding text, the increased turbulence correlation magnitude can also be interpreted as indicating that the bulk compression and streamline convergence act as a forcing function to increase the magnitude of the turbulent shear stress. As the clump moves up, i.e., $\Delta v > 0$, it will cross successive compression waves in an upstream orientation, i.e., the boundary layer experiences more compression as the wall is approached. Hence, neglecting the boundary-layer effects, $\Delta u < 0$ as a result of the compression. Thus, both the mean velocity gradient and compression act as forcing functions that tend to generate a positive Reynolds shear stress. Therefore, the turbulent shear-stress values should have increased over those for the zero-pressure-gradient flow.

The present data are consistent with the 100% (or twofold) increase for the model II curved-wall results of Jayaram et al.,[18] which were obtained using hot-wire anemometry. To compare the overall strengths of the pressure gradient, Eq. (1) was evaluated using their published data.[18] Thus, $I_T/(L_i/\delta_0)_T = 0.09$ compared to the value of 0.1 for the present case (see Table 3). Hence, the agreement in trends between the two studies was expected. Even though the individual impulses were different, the new parameter was very similar between the two studies. It is also interesting to note that the Reynolds numbers differed by a factor of 6.5. The k-ω model underpredicted the shear-stress magnitudes (Fig. 9) by roughly 50%.

The turbulent shear-stress results for the favorable-pressure-gradient region of the CPG model indicated that the levels had returned to values similar in magnitude to the incoming boundary layer, although a slight overshoot did remain over the upper portion of the boundary layer. The slight overshoot was a result of the upper portion of the boundary layer experiencing the full compression, but only a portion of the following expansion. Hence, based on the forcing function notions described earlier, it was expected that the shear-stress levels would be closer to the incoming boundary-layer levels near the wall where the flow has experienced almost equal and opposite expansion and compression waves, i.e., the change in axial momentum as a fluid clump moves in the positive transverse direction is relatively similar to that of the incoming boundary layer. However, in the outer region of the boundary layer, the clumps were still traversing across a portion of the compression wave. Qualitatively, these data agreed with the findings of Smith and Smits,[4] where the turbulent shear-stress levels returned to the upstream values at the exit of the successive pressure gradients (summarized in Table 3). The CFD shear-stress predictions (Fig. 9) were about 70% higher than the data.

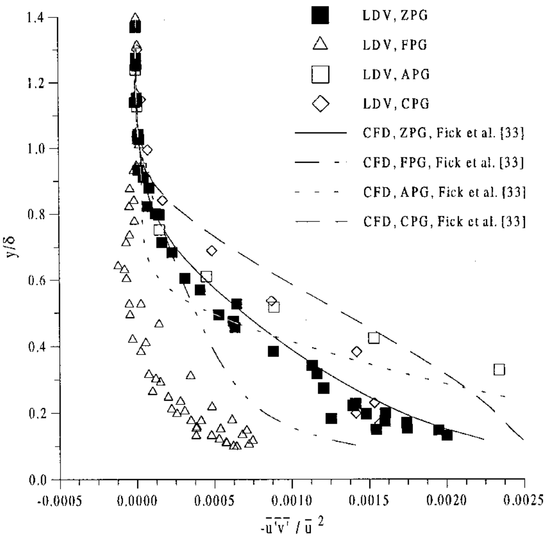

Fig. 9 Kinematic turbulent shear-stress profiles.

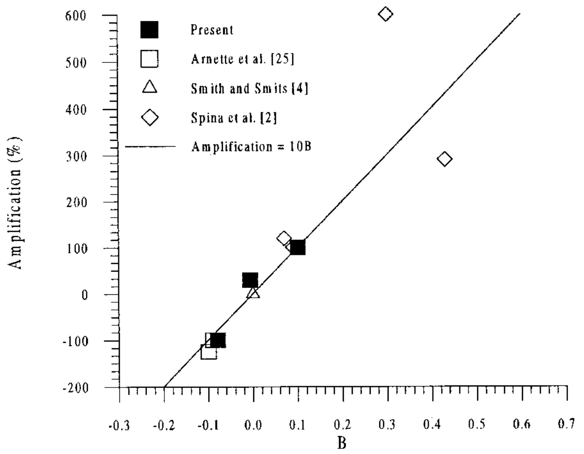

Fig. 10 Turbulent shear-stress amplification—new pressure gradient parameter correlation.

Although it is not suggested that the new parameter is representative of the flow physics, the data summarized in Table 3 do suggest a reasonable empirical correlation, even for combined-pressure gradient flows. The amplifications are plotted as a function of the new pressure gradient parameter B in Fig. 10. For the relatively mild pressure gradients summarized in Table 3, the peak amplification is about 10 times the parameter [Eq. (1)]; i.e., $(\tau_{xt}^{T} - \tau_{xy}^{0})/\tau_{xy}^{0} \approx 10B$. However, as the strength increases, the scatter seems to increase. For example, $B = 0.43$ for the model I curved-wall results summarized in Refs. 2 and 4, the amplification of the Reynolds shear stress was 290%. The correlation would predict a peak amplification of 430%. On the other hand, the model IV amplification was 600% for $B = 0.3$. Also, as $B \rightarrow \infty$ (i.e., $L_i = 0$), the amplification remains finite. For example, the 8- and 16-deg ramp data summarized in Refs. 2 and 4 had finite amplifications of 290 and 550%, respectively. Similarly, the 7- and 14-deg corner expansion data of Arnette et al.[25] had finite amplifications at nominally -110 and -130%, respectively. This indicates that an effective interaction length caused by the viscous effects is likely to be present. This may also explain the rather large scatter in Fig. 10 for the rapidly applied strong adverse-pressure gradients ($B > 0.3$), where the boundary-layer thickness was relatively large compared to the interaction length.

Conclusions

A detailed experimental investigation of the turbulent shear stresses for a supersonic boundary layer subjected to pressure-gradient-driven distortions was performed using two-component LDV. Four pressure-gradient flows were examined: a nominally zero-pressure-gradient case for comparative purposes ($M = 2.8$, $Re_\theta = 11{,}000$, $\beta = 0.02$); a favorable-pressure gradient ($M = 2.9$, $Re_\theta = 15{,}000$, $\beta = -0.5$); an adverse-pressure gradient ($M = 2.7$, $Re_\theta = 12{,}000$, $\beta = 0.9$); and a successive-pressure gradient ($M = 2.5$, $Re_\theta = 12{,}000$, $\beta = -1.0$ following a region of $\beta = 0.9$). For the adverse-pressure gradient, the turbulent shear-stress levels were amplified by 70–100%. For the favorable-pressure gradient, a 70–100% decrease was observed. For the combined-pressure gradient, the shear stresses returned to values similar to the zero-pressure gradient flow. A pressure-gradient parameter was defined, and found to correlate well with the peak amplification of the turbulent shear stresses. Previously reported data were also found to adhere to the same empirical correlation. It was also postulated that the shear-stress amplifications were in part the result of the nonuniform bulk dilatation and streamline divergence impressing a forcing function that affected the statistical $\overline{u'v'}$ correlation. The combined-pressure gradient flow demonstrated that the turbulent structure adjusted relatively rapidly to the distortion. The numerical simulations of the mean velocity obtained with a k-ω turbulence model were found to agree with the present data. However, with the exception of the zero-pressure-gradient flow, the magnitude of the turbulent shear stress was not accurately reproduced.

Acknowledgment

The authors gratefully acknowledge James McMichael of the U.S. Air Force Office of Scientific Research for sponsoring this work.

References

[1]Bradshaw, P., "The Effect of Mean Compression or Dilatation on the Turbulence Structure of Supersonic Boundary Layers," *Journal of Fluid Mechanics*, Vol. 63, Pt. 3, 1974, pp. 449–464.

[2]Spina, E., Smits, A., and Robinson, S., "The Physics of Supersonic Turbulent Boundary Layers," *Annual Review of Fluid Mechanics*, Vol. 26, 1994, pp. 287–319.

[3]Settles, G., and Dodson, L, "Supersonic and Hypersonic Shock/Boundary Layer Interaction Database," *AIAA Journal*, Vol. 32, No. 7, 1994, pp. 1377–1383.

[4]Smith, D., and Smits, A., "The Effects of Streamline Curvature and Pressure Gradient on the Behavior of Turbulent Boundary Layers in Supersonic Flow," AIAA Paper 94-2227, June 1994.

[5]Morkovin, M., "Effects of Compressibility on Turbulent Flows," *The Mechanics of Turbulence*, AGARD, Gordon and Breach, New York, 1961, pp. 368–380.

[6]Morkovin, M., "Effects of High Acceleration on a Turbulent Supersonic Shear Layer," *Proceedings of the 1955 Heat Transfer and Fluid Mechanics Inst.*, Vol. 4, 1955, pp. 1–17.

[7]Miller, R., Dotter, J., Bowersox, R., and Buter, T., "Compressible Turbulence Measurements in Supersonic Boundary Layers with Favorable and Adverse Pressure Gradients," *Transitional and Turbulent Compressible Flows*, edited by L. D. Kral, E. F. Spina, and C. Arakawa, Book G00974, FED.-Vol. 224, American Society of Mechanical Engineers, New York, 1995, pp. 193–200.

[8]Bowersox, R., and Buter, T., "Mass-Weighted Turbulence Measurements in a Mach 2.9 Boundary Layer Including Mild Pressure Gradients," *AIAA Journal*, Vol. 34, No. 12, 1996, pp. 2479–2483.

[9]Hayakawa, K, Smits, A., and Bogdonoff, S., "Hot-Wire Investigation of an Unseparated Shock-Wave/Boundary Layer Interaction," *AIAA Journal*, Vol. 22, 1984, pp. 579–585.

[10]Smits A., Young, S., and Bradshaw, P., "The Effects of Short Regions of High Surface Curvature on Turbulent Boundary Layers," *Journal of Fluid Mechanics*, Vol. 94, Sept. 1979, pp. 209–242.

[11]Waltrup, P., and Schetz, J., "Supersonic Turbulent Boundary Layer Subjected to Adverse Pressure Gradients," *AIAA Journal*, Vol. 11, No. 1, 1973, pp. 50–57.

[12]Lewis, J., Gran, R., and Kubota, T., "An Experiment on the Adiabatic Compressible Turbulent Boundary Layer in Adverse and Favorable-Pressure-Gradients," *Journal of Fluid Mechanics*, Vol. 51, Jan. 1972, pp. 657–672.

[13]Kussoy, M., Horstman, C., and Archarya, M., "An Experimental Documentation of the Pressure Gradient and Reynolds Number Effects on Compressible Turbulent Boundary Layers," NASA TM 78-488, Dec. 1978.

[14]Fernando, E., and Smits, A., "A Supersonic Turbulent Boundary Layer in an Adverse-Pressure-Gradient," *Journal of Fluid Mechanics*, Vol. 211, Feb. 1990, pp. 285–307.

[15]Smith, D., "The Effects of Successive Distortion on a Turbulent Boundary Layer in a Supersonic Flow," Ph.D. Dissertation, Princeton Univ., Princeton, NJ, 1993.

[16]Van Driest, E., "Turbulent Boundary Layer in Compressible Fluids," *Journal of the Aeronautical Sciences,* Vol. 18, No. 3, 1951, pp. 145–160.

[17]Thomann, H., "The Effects of Streamwise Wall Curvature on Heat Transfer in Turbulent Boundary Layers," *Journal of Fluid Mechanics*, Vol. 33, July 1968, pp. 283–292.

[18]Jayaram, M., Taylor, M., and Smits, A., "The Response of a Compressible Turbulent Boundary Layer to Short Regions of Concave Surface Curvature," *Journal of Fluid Mechanics*, Vol. 175, Feb. 1987, pp. 343–362.

[19]Smits, A., and Muck, K., "Experimental Study of Three Shock Waver/Turbulent Boundary Layer Interactions," *Journal of Fluid Mechanics,* Vol. 182, Sept. 1987, pp. 291–314.

[20]Donovan, J., Spina, E., and Smits, A., "The Structure of Supersonic Turbulent Boundary Layers Subjected to Concave Surface Curvature," *Journal of Fluid Mechanics*, Vol. 259, Jan. 1994, pp. 1–24.

[21]Narasimha, R., and Sreenivasan, K., "Relaminarization in Highly Accelerated Turbulent Boundary Layers," *Journal of Fluid Mechanics*, Vol. 61, Oct.–Dec. 1973, pp. 417–447.

[22]Smith, D., and Smits, A., "The Rapid Expansion of a Turbulent Boundary Layer in a Supersonic Flow," *Theoretical Computational Fluid Dynamics*, Vol. 2, 1991, pp. 319–328.

[23]Dussauge, J., and Gaviglio, J., "The Rapid Expansion of a Supersonic Turbulent Flow: The Role of Bulk Dilatation," *Journal of Fluid Mechanics*, Vol. 174, Jan. 1987, pp. 81–112.

[24]Johnson, A., "Laminarization and Retransition of Turbulent Boundary Layers in Supersonic Flow," Ph.D. Dissertation, Yale Univ., New Haven, CT, 1993.

[25]Arnette, S., Samimy, M., and Elliot, G., "The Effects of Expansion Regions on the Turbulence Structure of Compressible Boundary Layers," AIAA Paper 96-0656, Jan. 1996.

[26]Zheltovodov, A., Trofimov, V., Shilein, E., and Yakovlev, V., "An Experimental Documentation of Supersonic Turbulent Flows in the Vicinity if Sloping Forward and Back Facing Steps," Inst. of Theoretical and Applied Mechanics, Siberian Div. of the USSR Academy of Sciences, TPM Rept. 2013, Novosibirsk, Russia, 1990.

[27]Wilcox, D., *Turbulence Modeling for CFD*, DCW Industries, La Cañada, CA, 1993.

[28]Hale, C., "Experimental Investigation of a Supersonic Boundary Layer with Adverse-Pressure Gradient," M.S. Thesis, U.S. Air Force Inst. of Technology, AFIT/GAE/ENY/95D-12, Wright–Patterson AFB, OH, 1995.

[29]Luker, J., "Experimental Investigation of a Supersonic Boundary Layer Including Favorable-Pressure-Gradient Effects," M.S. Thesis, Air Force Inst. of Technology, AFIT/GAE/ENY/95D-16, Wright–Patterson AFB, OH, 1995.

[30]Schetz, J., *Boundary Layer Analysis*, Prentice–Hall, Englewood Cliffs, NJ, 1993.

[31]White, F., *Viscous Fluid Flow,* McGraw–Hill, New York, 1991.

[32]Clauser, F. H., "Turbulent Boundary Layers in Adverse-Pressure Gradients," *Journal of the Aeronautical Sciences*, Vol. 21, Feb. 1954, pp. 91–108.

[33]Fick, E., Buter, T., and Gaitonde, D., "Numerical Simulation of Supersonic Turbulent Boundary Layer with Mild Pressure Gradient," AIAA Paper 96-2059, June 1996.

[34]Robinson, S. K., Seegmiller, H. L., and Kussoy, M. I., "Hot-Wire and Laser Doppler Anemometer Measurements in a Supersonic Boundary Layer," AIAA Paper 83-1723, June 1983.

[35]Elena, M., and LeCharme, J., "Experimental Study of a Supersonic Turbulent Boundary Layer Using a Laser Doppler Anemometer," *Journal of Theoretical and Applied Mechanics*, Vol. 7, No. 2, 1988, pp. 175–190.

[36]Johnson, D., and Rose, W., "Laser Velocimeter and Hot-Wire Anemometer Comparison in a Supersonic Boundary Layer," *AIAA Journal*, Vol. 13, No. 4, 1975, pp. 512–515.

[37]Klebanoff, P. S., "Characteristics of Turbulence in a Boundary Layer with Zero-Pressure-Gradient," NACA Rept. 1247, May 1955.